

Deconfining disordered phase in two-dimensional quantum link models

Lorenzo Cardarelli,¹ Sebastian Greschner,² and Luis Santos¹

¹*Institut für Theoretische Physik, Leibniz Universität Hannover, Appelstr. 2, DE-30167 Hannover, Germany*

²*Department of Quantum Matter Physics, University of Geneva, CH-1211 Geneva, Switzerland*

(Dated: February 19, 2020)

We explore the ground-state physics of two-dimensional spin-1/2 $U(1)$ quantum link models, one of the simplest non-trivial lattice gauge theories with fermionic matter within experimental reach for quantum simulations. Whereas in the large mass limit we observe Néel-like vortex-antivortex and striped crystalline phases, for small masses there is a transition from the striped phases into a disordered phase whose properties resemble those at the Rokhsar-Kivelson point of the quantum dimer model. This phase is characterized on ladders by boundary Haldane-like properties, such as vanishing parity and finite string ordering. Moreover, from studies of the string tension between gauge charges, we find that whereas the striped phases are confined, the novel disordered phase present clear indications of being deconfined. Our results open exciting perspectives of studying highly non-trivial physics in quantum simulators, such as spin-liquid behavior and confinement-deconfinement transitions, without the need of explicitly engineering plaquette terms.

Driven by tremendous progresses in the manipulation and control of ultracold quantum gases, this field is entering the era of the quantum simulation of lattice gauge theories (LGTs) [1], with the long term goal of studying open problems of the early universe, dense neutron stars, nuclear physics or condensed-matter physics [2–4]. Many theoretical proposals [5–18] and recent seminal experiments with trapped ions [19], quantum dimer models in Rydberg-atoms-arrays [20], lattice modulation techniques [21–23], or atomic mixtures [24] have shown first building-blocks of dynamical gauge fields and quantum link models (QLMs), a generalization of LGT to spin-like link-variables [25]. However, the implementation of some building blocks of LGT, such as the ring-exchange corresponding to magnetic field dynamics in analogue implementations of quantum electrodynamics, requires further theoretical and experimental breakthroughs, although there has been progress on isolated plaquettes [26] and recent promising proposals [27, 28].

In this paper we show how already the simplest mid-term experimental realizations, without plaquette terms, may be able to explore a wide area of non-trivial phenomena of LGTs. In particular, we report in this Letter that the two-dimensional (2D) QLM is characterized by the emergence of a quantum phase transition between confined crystalline phases and an exotic deconfined disordered phase with certain resemblance to Rokhsar-Kivelson (RK) states [29] or resonating valence bond liquids [30–33]. Hence, these relatively simple systems provide a pristine test-bed for the study of highly non-trivial physics, such as spin liquids, confinement-deconfinement transitions, and exotic dynamical or thermalization properties [20, 34, 35], such as the formation of quantum many-body scars in constrained systems [36] and their fundamental link to confinement. Interestingly, QLMs may be experimentally realized in quantum gases within the next years. Whereas several proposals using Fermi-Bose mixtures have been reported [8, 9, 11, 14, 15, 17, 24],

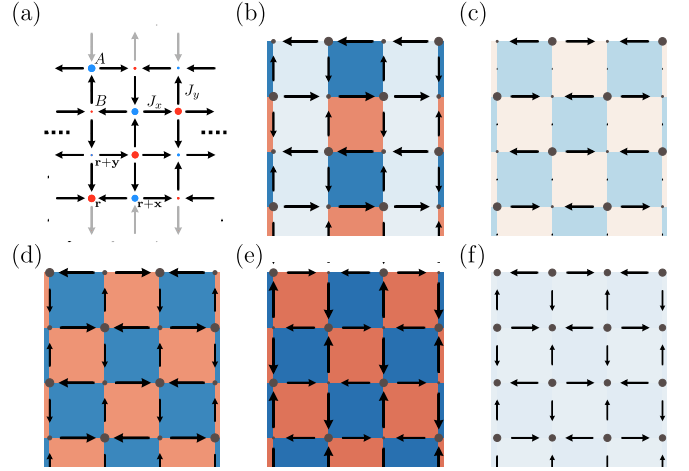


FIG. 1. (a) Sketch of the QLM model on a square ladder (gray spins depict staggered boundary conditions) or on a torus (associating opposite gray spins at the two edges). (b-f) Sketches of the phases discussed in the text: for $\mu = 0.8$ striped phases (b) $J_y = 2.4J_x$ (Sy), (c) $J_y = 0.2J_x$ (Sx); for $\mu = -0.8$ vortex-antivortex phases (d) $J_y = 2.4J_x$ (VA) (e) $J_y = 0.2J_x$ (VA'), and the (f) disordered/deconfined D phase for $\mu = 0$ and $J_x = J_y$. The size of the bullets depicts $\langle n_r \rangle$, the arrow size $\langle S_{r,r'}^z \rangle$, and the plaquette colors the vorticity $\langle Q_r \rangle$. The arrow sizes of (f) has been scaled up by a factor of 2 for clarity.

we recently discussed [16] a minimalistic realization of QLMs with a single fermionic species that simulates the spin-1/2 links using multi-orbital physics in optical superlattices [37]. We note, however, that the latter may be analogously replaced by hyper-fine or spatial degrees of freedom allowing for a large flexibility of the proposal.

2D QLM.— We consider in the following a QLM on a square lattice described by the Hamiltonian

$$H = - \sum_{\mathbf{r}, \mathbf{r}'} J_{\mathbf{r}, \mathbf{r}'} \left(\psi_{\mathbf{r}}^\dagger S_{\mathbf{r}, \mathbf{r}'}^+ \psi_{\mathbf{r}'} + \text{h.c.} \right) + \sum_{\mathbf{r}} \mu_{\mathbf{r}} n_{\mathbf{r}}, \quad (1)$$

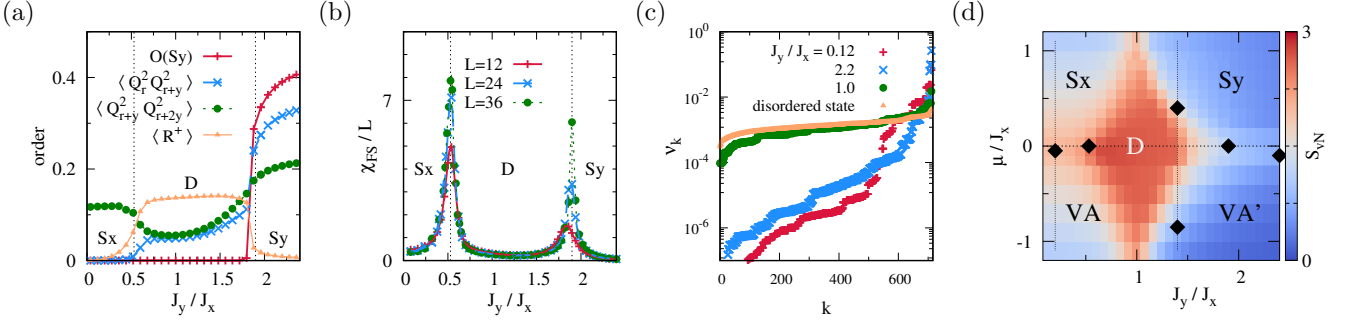


FIG. 2. Four-leg cylinder at $\mu = 0$: (a) Nearest and next-nearest neighbor flippability correlations, staggered flippability $O(Sy) = \sum_{\mathbf{r}} (-)^x \langle Q_{\mathbf{r}}^2 \rangle$, as well as the expectation value of the ring-exchange $\langle R_{\mathbf{r}}^+ \rangle$. (b) Fidelity susceptibility with $L = 12, 24$ and 36 rungs. (c) Local Hilbert space distribution ν_k of the central rung (see text). (d) Sketched phase diagram of the QLM. Color codes depict the von-Neumann bipartite entanglement entropy S_{vN} of the central rung. Points depicts the estimated phase transition points, by extrapolating the peak positions of the fidelity susceptibility evaluated along the cuts indicated by the dotted lines (DMRG data).

where $\psi_{\mathbf{r}}^\dagger$ is the fermionic operator at site \mathbf{r} , and $n_{\mathbf{r}} = \psi_{\mathbf{r}}^\dagger \psi_{\mathbf{r}}$. In our case the gauge field is given by spin-1/2 operators $S_{\mathbf{r},\mathbf{r}'}$ placed at the link between two neighbouring sites \mathbf{r} and \mathbf{r}' . The amplitudes $J_{\mathbf{r},\mathbf{r}+\mathbf{x}} = J_x$ and $J_{\mathbf{r},\mathbf{r}+\mathbf{y}} = J_y$ characterize, respectively, the hops along the x and y directions (Fig. 1 (a)). We enforce at each site the Gauss law $[H, G_{\mathbf{r}}] = 0$ with $G_{\mathbf{r}} = \varepsilon_{\mathbf{r}} - n_{\mathbf{r}} + \sum_{\mathbf{k} \in \mathbf{x}, \mathbf{y}} (S_{\mathbf{r},\mathbf{r}+\mathbf{k}}^z - S_{\mathbf{r},\mathbf{r}-\mathbf{k}}^z)$, with $\varepsilon_{\mathbf{r} \in A} = 1$ and $\varepsilon_{\mathbf{r} \in B} = 0$. The staggered potential, $\mu_{\mathbf{r} \in A} = \mu$ and $\mu_{\mathbf{r} \in B} = -\mu$ can be interpreted as the mass of particles on B sites and anti-particles on A sites.

We focus on the ground-states of the QLM at half fermion filling and gauge vacuum ($G_{\mathbf{r}} = 0$) on square ladders and cylinders. We study up to $L_x = 100$ rungs and $L_y = 4$ legs by means of density matrix renormalization group (DMRG) techniques [38] adapted to the local gauge symmetry [39–42]. We introduce at this point the ring-exchange operators $R_{\mathbf{r}}^+ = S_{\mathbf{r},\mathbf{r}+\mathbf{x}}^+ S_{\mathbf{r}+\mathbf{x},\mathbf{r}+\mathbf{x}+\mathbf{y}}^- S_{\mathbf{r}+\mathbf{x}+\mathbf{y},\mathbf{r}+\mathbf{y}}^+ S_{\mathbf{r}+\mathbf{y},\mathbf{r}}^+$ and $R_{\mathbf{r}}^- = (R_{\mathbf{r}}^+)^{\dagger}$. These operators characterize plaquette states: $R_{\mathbf{r}}^-$ ($R_{\mathbf{r}}^+$) flips a vortex (antivortex) into an antivortex (vortex), being zero otherwise, and $Q_{\mathbf{r}} = (R_{\mathbf{r}}^+ R_{\mathbf{r}}^- - R_{\mathbf{r}}^- R_{\mathbf{r}}^+) = 1$ (-1) for vortex (antivortex) and $Q_{\mathbf{r}} = 0$ otherwise [43].

Large mass limit.— First insights are obtained from the limit $|\mu| \gg J_{x,y}$, which, in contrast to the two-leg QLM [44], is different for $\mu > 0$ and $\mu < 0$. For $\mu > 0$, particles are pinned in B sites (Figs. 1 (b) and (c)). Local states are characterized by the expectation value of two spin-1 operators, $S_{\mathbf{k}}^z(\mathbf{r}) = S^z(\mathbf{r}-\mathbf{k},\mathbf{r}) + S^z(\mathbf{r},\mathbf{r}+\mathbf{k})$, with $\mathbf{k} = \mathbf{x}, \mathbf{y}$. For $J_x < J_y$, second-order terms select a ground-state manifold of two states with $S_y^z(\mathbf{r}) = 0$. Fourth-order ring-exchange $\propto J_x^2 J_y^2 / |\mu|^3$ [16] favors a configuration of columns of flippable vortex-antivortex and non-flippable plaquettes (Fig. 1 (b)). We denote this striped phase Sy. In a 2D model, a corresponding striped phase Sx of alternating flippable and non-flippable rows of plaquettes is expected for $J_y < J_x$. However, on the finite-size cylinders we study, the trans-

lational symmetry along the y direction results in blurred spin averages (Fig. 1 (c)). Correlations of the flippability operators reveal the Sx character (Fig. 2 (a)): whereas $\langle Q_{\mathbf{r}}^2 Q_{\mathbf{r}+\mathbf{y}}^2 \rangle$ vanishes, $\langle Q_{\mathbf{r}}^2 Q_{\mathbf{r}+2\mathbf{y}}^2 \rangle$ remains finite. Staggered boundary spins stabilize the Sx ordering in ladders [44].

For large negative mass, $-\mu \gg J_{x,y}$, particles are pinned to the A-sites, reducing the local Hilbert space to a six-dimensional manifold of spin configurations satisfying Gauss' law. Second-order processes favor states with $\langle S_x^z(\mathbf{r}) \rangle = \langle S_y^z(\mathbf{r}) \rangle = 0$, leading to a checkerboard ground-state pattern of vortex-antivortex (VA) plaquettes (Figs. 1 (d) and (e)). For $J_x < J_y$ we dub this phase VA, and VA' for $J_y < J_x$. These two phases are uniquely defined and do not exhibit any spontaneously broken translational symmetry like in a Néel-like phase.

Emerging disordered phase.— At low μ particle fluctuations become important, leading to a particularly intriguing physics. For $\mu \sim 0$ we observe three distinct phases as a function of J_y/J_x , as can be seen in Fig. 2 (b) for the four-leg cylinder by the distinct diverging peaks in the fidelity susceptibility $\chi_{FS} = \lim_{J_y \rightarrow J'_y} \frac{-2 \ln |\langle \Psi_0(J_y) | \Psi_0(J'_y) \rangle|}{(J_y - J'_y)^2}$, where $|\Psi_0\rangle$ is the ground-state wave-function. We observe a similar behavior for three- and four-leg ladders [44]. Whereas for $\mu = 0$ for $J_y \ll J_x$ ($J_y \gg J_x$) the system is in the Sx (Sy) phase, for $J_x \sim J_y$ an intermediate gapped phase occurs characterized by vanishing $\langle Q_{\mathbf{r}} \rangle$ and $\langle Q_{\mathbf{r}}^2 \rangle$, but a large expectation value of the ring-exchange $\langle R_{\mathbf{r}}^+ \rangle$.

A crucial insight on the physics of the intermediate phase is provided by the analysis of the reduced density matrix $\rho_c = \text{Tr} |\Psi_0\rangle \langle \Psi_0|$ for the central rung (where the trace runs over all other rungs) in the (Fock-like) eigenbasis ϕ_k of $S_{\mathbf{r},\mathbf{r}'}$ and $n_{\mathbf{r}}$. In Fig. 2 (c) we show its diagonal elements $\nu_k = \langle \phi_k | \rho_c | \phi_k \rangle$, an effective local Hilbert space distribution, sorted by amplitude, for the case of a four-leg cylinder. The Sx and Sy phases are strongly localized in Fock space, i.e. ν_k has most weight for few basis

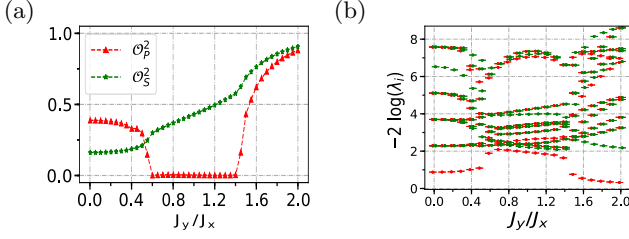


FIG. 3. (a) Parity and string order along the boundary legs of a four-leg ladder, obtained using DMRG for $L_x = 100$ rungs and $\mu = 0$; (b) largest eigenvalues of the entanglement spectrum, obtained after dividing the system into two parts along the central rung.

states. The intermediate phase, however, exhibits a drastically different, much flatter distribution, where many local Fock states contribute with similar weight. The disordered character of the intermediate phase is also witnessed by the entanglement entropy $S_{vN} = -\text{Tr}(\rho_c \ln \rho_c)$, which we depict in Fig. 2 (d).

The intermediate phase thus closely resembles the Rokhsar-Kivelson (RK) point, which contains an equal superposition of all dynamically connected states. We also show in Fig. 2 (c) the corresponding distribution of ν_k for a classical RK state, which compares well to the ground state obtained by the DMRG simulation. We estimate the overlap between the two states to be 0.97 (see [44] for a more detailed comparison between the DMRG simulation of the intermediate phase and the classical RK state, which also reproduces the spin and density configuration pattern of Fig. 1 (f)). We hence characterize the intermediate gapped phase as a disordered (D) phase. Note, that due to the different Gauss' law on A and B sites, this phase still exhibits a slight particle imbalance between A and B sites, as well as finite link-variable expectation values, as shown in Fig. 1 (f).

Edge Haldane order.— We focus at this point on the edges of a QLM ladder, where the physics can be well understood from a mean-field-like strongly simplified 1D model in which we fix the upper boundary links for each site in a staggered configuration, and allow the lower spins to fluctuate with an amplitude J_y . Six local states are possible: $|\bar{0}_\pm\rangle = (|\uparrow^\circ\uparrow^\leftarrow\rangle \pm |\uparrow^\leftarrow\downarrow^\leftarrow\rangle)/\sqrt{2}$, $|\bar{0}_\pm\rangle = (|\uparrow^\circ\uparrow^\rightarrow\rangle \pm |\uparrow^\rightarrow\downarrow^\rightarrow\rangle)/\sqrt{2}$, $|\alpha\rangle = |\uparrow^\circ\downarrow^\leftarrow\rangle$, and $|\beta\rangle = |\uparrow^\leftarrow\downarrow^\rightarrow\rangle$. Gauss' law imposes further restrictions on the allowed sequence of these local states: 0 may be followed at its right by 0 or β ($0 \rightarrow 0, \beta$); $\bar{0} \rightarrow \bar{0}, \alpha$; $\alpha \rightarrow \beta, 0$; and $\beta \rightarrow \alpha, \bar{0}$ (we remove the \pm index). By construction, Gauss' law enforces a Néel-like order of α and β states diluted by an arbitrary number of intermediate 0 or $\bar{0}$ states. The model Hamiltonian, given by

$$H_{1D} = -J_x \sum_x \psi_x^\dagger S_{x,x+1}^+ \psi_{x+1} - J_y \sum_x \psi_x^\dagger S_x^+ + \text{H.c.} \quad (2)$$

exhibits three ground-state phases (here we neglect a staggered potential term). For $J_y \ll J_x$ the ground state is $\cdots |\alpha\rangle |\beta\rangle |\alpha\rangle |\beta\rangle \cdots$, whereas for $J_y \gg J_x$ the states $\cdots |0_-\rangle |0_-\rangle \cdots$ and $\cdots |\bar{0}_-\rangle |\bar{0}_-\rangle \cdots$ have the lowest energy. Interestingly, for $J_x \sim J_y$ an intermediate phase with Haldane-like diluted Néel order emerges, that resembles the SPT phase of Ref. [16]. We may describe this intermediate phase by a minimal AKLT-like [45] state with a two-fold degenerate entanglement spectrum and a non-vanishing string order $\mathcal{O}_S^2 = \lim_{|x-x'| \rightarrow \infty} \langle S_x^z e^{i\pi \sum_{x < k < x'} S_k^z} S_{x'}^z \rangle$, while parity order $\mathcal{O}_P^2 = \lim_{|x-x'| \rightarrow \infty} \langle e^{i\pi \sum_{x < k < x'} S_k^z} \rangle$ is exponentially suppressed [44].

While being a drastically simplified description, it captures essential ingredients of ladder QLMs. In particular, fixing in a ladder the boundary spins to a staggered configuration enforces the dilute Néel order on the boundary leg. We, hence, plot in Fig. 3 (a) the string- and parity order measured along the boundary leg of a 4-leg ladder. Indeed the D phase is characterized by a finite string order and a vanishing parity order, resembling closely the SPT phase discussed for the above mentioned 1D model or the two-leg QLM of Ref. [16]. However, for $L_y > 2$ the parity order remains finite in the D phase if measured on the inner legs, and the phase is not topological. The entanglement spectrum is no longer strictly two-fold degenerate. Interestingly, however, we observe a robust gap in the entanglement spectrum of the D phase between a low-lying manifold and the rest.

String tension.— Finally, we discuss the properties of gauge charges on top of the vacuum state. We insert two charges by locally adjusting Gauss' law to $G_{\mathbf{r}} = \pm 1$ on two sites separated by a distance L_D in x -direction, and study the string formation for the case of a four-leg cylinder. Example configurations are shown in Figs. 4 (a)-(c) for Sy, Sx and D phases after subtracting the spin and fermion configuration of the charge-free system. Comparing the energy $E(L_D)$ with the energy E_0 of the charge-free state, we obtain the string tension, $\mathcal{T}(L_D) = E(L_D) - E_0$ (Fig. 4 (d)), which characterizes the confining properties [40].

Only Sy shows a clear string formation (Fig. 4 (a)). The tension increases linearly in a staggered way due to the broken symmetry, as depicted in Fig. 4(d). This is a clear signature of the confinement of excitations. For the Sx phase the increase of potential energy is also linear and very large compared to the other phases. Here, however, after some distance the string breaks and is wrapped around the cylinder in y -direction (see Fig. 4 (b)). Also the string tension flattens after this point as shown in Fig. 4 (d) for $J_y/J_x = 0.4$. Interestingly, the two charges become, hence, effectively deconfined due to the finite size of the system in y -direction.

In the D phase the tension grows slowly with L_D and potentially finally saturates, indicating charge deconfinement. Contrary to the Sx phase we observe in Fig. 4 (c)

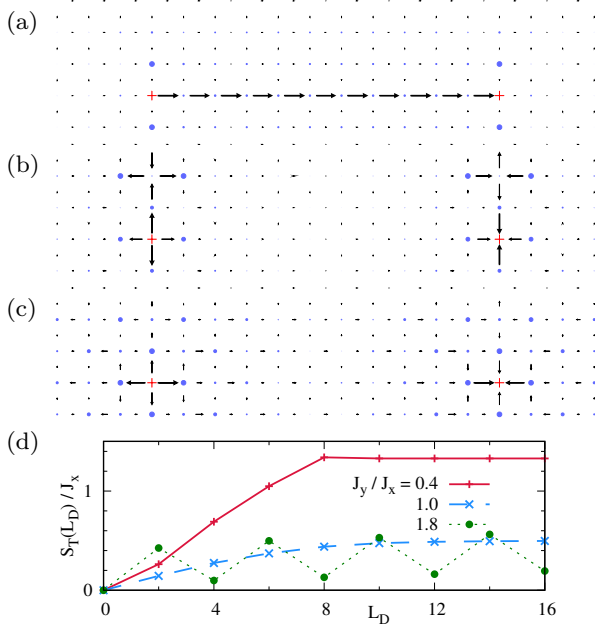


FIG. 4. (a) Average fermionic density and bond configuration of two charges at a distance of $L_D = 12$ sites, after subtracting the charge-free configuration. We employ DMRG for a cylinder with $L_y = 4$ legs and $L = 36$ rungs and $\mu = 0.4J_x$. (a) Sy phase ($J_y = 1.8J_x$), (b) Sx phase ($J_y = 0.4J_x$), (c) D phase ($J_y = J_x$). (d) String tension S_T as a function of the distance between the defects L_D .

the formation of a symmetric broad but localized perturbation of the spin and charge background around the defects. Even though due to the limited system size we cannot distinguish the saturation of the string tension from a further slow (e.g. logarithmic) growth, these results show that Sx, Sy and D phases exhibit drastically different confinement and deconfinement properties.

Conclusions.— We studied the ground state of a 2D spin-1/2 QLM, which may be realizable in quantum gas lattice gauge simulators in the foreseeable future. Despite the absence of plaquette terms, 2D QLMs are characterized by a highly nontrivial physics. As a main result, we have found an emergent deconfined disordered phase for $\mu \sim 0$ and $J_x \sim J_y$, which closely resembles an RK phase. On finite ladder systems with staggered boundary spins this phase exhibits Haldane-like ordering at the edge legs. While being limited to small transversal lengths $L_y \leq 4$, the observed features qualitatively remain robust over two-, three- and four-leg ladders and four-leg cylinders, strongly hinting that the intermediate disordered phase may survive in more general 2D lattices, which might inspire further numerical efforts in this direction.

Our results open the interesting possibility to study a wealth of phenomena such as deconfinement-confinement transition and RVB-like physics in quantum gas lattice gauge simulators, without the need of explicitly realizing ring-exchange and RK terms. The dynamics of these

systems may be particularly interesting. Further experimental and theoretical studies should reveal the potentially unconventional thermalization properties [35, 36] of constrained systems with fermionic matter.

We thank Alessio Celi and Marcello Dalmonte for enlightening discussions. S. G. acknowledges support by the Swiss National Science Foundation under Division II. L. C. and L. S. thank the support of the German Research Foundation Deutsche Forschungsgemeinschaft (Project No. SA 1031/10-1 and the Excellence Cluster QuantumFrontiers). Simulations were carried out on the cluster system at the Leibniz University of Hannover and the boabab cluster of the University of Geneva.

-
- [1] K. G. Wilson, Phys. Rev. D **10**, 2445 (1974).
 - [2] J. B. Kogut, Rev. Mod. Phys. **55**, 775 (1983).
 - [3] M. Levin and X.-G. Wen, Rev. Mod. Phys. **77**, 871 (2005).
 - [4] U.-J. Wiese, Annalen der Physik **525**, 777 (2013).
 - [5] J. I. Cirac, P. Maraner, and J. K. Pachos, Phys. Rev. Lett. **105**, 190403 (2010).
 - [6] E. Zohar and B. Reznik, Phys. Rev. Lett. **107**, 275301 (2011).
 - [7] E. Kapit and E. Mueller, Phys. Rev. A **83**, 033625 (2011).
 - [8] E. Zohar, J. I. Cirac, and B. Reznik, Phys. Rev. Lett. **109**, 125302 (2012).
 - [9] D. Banerjee, M. Dalmonte, M. Müller, E. Rico, P. Stebler, U.-J. Wiese, and P. Zoller, Phys. Rev. Lett. **109**, 175302 (2012).
 - [10] E. Zohar, J. I. Cirac, and B. Reznik, Phys. Rev. Lett. **110**, 055302 (2013).
 - [11] D. Banerjee, M. Bögli, M. Dalmonte, E. Rico, P. Stebler, U.-J. Wiese, and P. Zoller, Phys. Rev. Lett. **110**, 125303 (2013).
 - [12] E. Zohar, J. I. Cirac, and B. Reznik, Phys. Rev. Lett. **110**, 125304 (2013).
 - [13] L. Tagliacozzo, A. Celi, P. Orland, M. Mitchell, and M. Lewenstein, Nat. Comm. **4** (2013).
 - [14] K. Stannigel, P. Hauke, D. Marcos, M. Hafezi, S. Diehl, M. Dalmonte, and P. Zoller, Phys. Rev. Lett. **112**, 120406 (2014).
 - [15] V. Kasper, F. Hebenstreit, M. Oberthaler, and J. Berges, Phys. Lett. B **760**, 742 (2016).
 - [16] L. Cardarelli, S. Greschner, and L. Santos, Phys. Rev. Lett. **119**, 180402 (2017).
 - [17] T. V. Zache, F. Hebenstreit, F. Jendrzejewski, M. K. Oberthaler, J. Berges, and P. Hauke, Quantum Science and Technology **3**, 034010 (2018).
 - [18] L. Barbiero, C. Schweizer, M. Aidelsburger, E. Demler, N. Goldman, and F. Grusdt, Science advances **5**, eaav7444 (2019).
 - [19] E. A. Martinez, C. A. Muschik, P. Schindler, D. Nigg, A. Erhard, M. Heyl, P. Hauke, M. Dalmonte, T. Monz, P. Zoller, and R. Blatt, Nature **534**, 516 (2016).
 - [20] H. Bernien, S. Schwartz, A. Keesling, H. Levine, A. Omran, H. Pichler, S. Choi, A. S. Zibrov, M. Endres, M. Greiner, V. Vuletic, and M. D. Lukin, Nature **551**, 579 EP (2017), article.
 - [21] L. W. Clark, B. M. Anderson, L. Feng, A. Gaj, K. Levin,

- and C. Chin, Phys. Rev. Lett. **121**, 030402 (2018).
- [22] F. Görg, K. Sandholzer, J. Minguzzi, R. Desbuquois, M. Messer, and T. Esslinger, Nature Physics **15**, 1161 (2019).
 - [23] C. Schweizer, F. Grusdt, M. Berngruber, L. Barbiero, E. Demler, N. Goldman, I. Bloch, and M. Aidelsburger, Nature Physics **15**, 1168 (2019).
 - [24] A. Mil, T. V. Zache, A. Hegde, A. Xia, R. P. Bhatt, M. K. Oberthaler, P. Hauke, J. Berges, and F. Jendrzejewski, arXiv preprint arXiv:1909.07641 (2019).
 - [25] S. Chandrasekharan and U.-J. Wiese, Nucl. Phys. B **492**, 455 (1997).
 - [26] H.-N. Dai, B. Yang, A. Reingruber, H. Sun, X.-F. Xu, Y.-A. Chen, Z.-S. Yuan, and J.-W. Pan, Nat. Phys. **13**, 1195 (2017).
 - [27] A. Celi, B. Vermersch, O. Viyuela, H. Pichler, M. D. Lukin, and P. Zoller, arXiv preprint arXiv:1907.03311 (2019).
 - [28] A. Bohrdt, A. Omran, E. Demler, S. Gazit, and F. Grusdt, arXiv preprint arXiv:1910.00023 (2019).
 - [29] D. S. Rokhsar and S. A. Kivelson, Phys. Rev. Lett. **61**, 2376 (1988).
 - [30] B. S. Shastry and B. Sutherland, Physica B+C **108**, 1069 (1981).
 - [31] P. W. Anderson, Science **235**, 1196 (1987).
 - [32] R. Moessner and S. L. Sondhi, Progress of Theoretical Physics Supplement **145**, 37 (2002).
 - [33] A. Ralko, M. Ferrero, F. Becca, D. Ivanov, and F. Mila, Phys. Rev. B **71**, 224109 (2005).
 - [34] M. Brenes, M. Dalmonte, M. Heyl, and A. Scardicchio, Phys. Rev. Lett. **120**, 030601 (2018).
 - [35] J. Feldmeier, F. Pollmann, and M. Knap, Phys. Rev. Lett. **123**, 040601 (2019).
 - [36] C. J. Turner, A. A. Michailidis, D. A. Abanin, M. Serbyn, and Z. Papić, Nat. Phys. **14**, 745 (2018).
 - [37] G. Wirth, M. Ölschläger, and A. Hemmerich, Nature Phys. **7**, 147 (2011).
 - [38] U. Schollwöck, Annals of Physics **326**, 96 (2011).
 - [39] M. Dalmonte and S. Montangero, Contemporary Physics **57**, 388 (2016).
 - [40] F. Tschirsich, S. Montangero, and M. Dalmonte, SciPost Phys. **6**, 28 (2019).
 - [41] N. Chepiga and F. Mila, SciPost Physics **6**, 033 (2019).
 - [42] We keep up to 300 DMRG states which shows sufficient convergence for the gapped phases described in the paper.
 - [43] Following the standard convention, we depict in our figures the spin S^z as $\uparrow (\rightarrow)$ and $\downarrow (\leftarrow)$ in y (x)-links. A vortex (antivortex) plaquette has a spin configuration up, up, down, down (down, down, up, up) starting with the spin at the left side and proceeding clockwise.
 - [44] See Supplementary Material, which includes Refs. [45–48], for detailed numerical results and extended data on the RK-states and string-tension calculations, and on the simplified 1D model of Eq. (2).
 - [45] I. Affleck, T. Kennedy, E. Lieb, and H. Tasaki, Phys. Rev. Lett. **59**, 799 (1987).
 - [46] F. Pollmann, A. M. Turner, E. Berg, and M. Oshikawa, Phys. Rev. B **81**, 064439 (2010).
 - [47] F. Pollmann and A. M. Turner, Phys. Rev. B **86**, 125441 (2012).
 - [48] F. Pollmann, E. Berg, A. M. Turner, and M. Oshikawa, Phys. Rev. B **85**, 075125 (2012).